Reaction channel contributions to proton scattering at 65 MeV

R. S. Mackintosh [*]

School of Physical Sciences, The Open University, Milton Keynes MK7 6AA, United Kingdom

N. Keeley[†]

National Centre for Nuclear Research, ul. Andrzeja Sołtana 7, 05-400 Otwock, Poland

Background: Well-established coupled channel (CC) and coupled reaction channel (CRC) processes make contributions to elastic scattering that are absent from local density folding models.

Purpose: To establish and characterize the contribution to the proton optical model potential (OMP) made by the coupling to neutron pickup channels, in particular the proton OMP for 65 MeV protons on ^{48}Ca and ^{40}Ca. Also to relate this contribution to results for ^{40}Ca at lower energies; to investigate the dynamical nonlocality of this contribution; to characterize the effect on the OMP of breakup of the deuteron.

Methods: CRC calculations of neutron pickup and CC calculations of collective states, provide the elastic channel S matrix S_{lj}. Inversion of S_{lj} produces a local potential that yields, in a single channel calculation, the elastic scattering observables from the CC/CRC calculation. Subtracting the bare potential yields a local and l-independent representation of the dynamical polarization potential, DPP. From the DPPs due to a selection of channel couplings the influence of dynamically generated nonlocality can be identified. The effect of coupling to the deuteron breakup continuum is also identified.

Results: For ^{40}Ca, coupling to pickup channels has an effect on observables somewhat weaker than that at 30 MeV, and much less than for pickup coupling for ^{48}Ca. The DPPs have similar general properties in each case, but are much larger in magnitude for ^{48}Ca. Subsequent breakup of the deuteron makes a large contribution to the DPP, and hence to the OMP. The formal DPPs due to pickup coupling exhibit dynamical nonlocality.

Conclusions: The DPPs challenge local density folding models for elastic scattering. The breakup of the deuteron must henceforth be included in calculations of the DPP due to neutron pickup in proton scattering. Pickup coupling effects are still substantial at 65 MeV. No smoothly varying global OMP could fit proton elastic scattering from both ^{40}Ca and ^{48}Ca.

I. INTRODUCTION

Previously, in Ref. [1] and references therein, we have shown that coupling to reaction and inelastic channels contributes to the proton optical model potential (OMP) in ways that are not represented in current folding models. In particular, folding model potentials require corrections that cannot be represented by a uniform renormalization. Among other effects, reaction channel coupling generates a systematic change in the rms radius of the real potential. As in earlier work, the key to determining the required corrections is to determine local potentials that give an exact representation of the elastic scattering S matrix, S_{lj}, when the processes of interest are active. In this way the changes in local potentials representing particular inelastic processes can be determined. This provides information concerning the dynamical polarization potential (DPP) arising from particular processes and suggests limitations of folding models that have no representation of such processes.

The present work exploits a remarkably comprehensive study of 65 MeV proton scattering from ^{40}Ca and ^{48}Ca, and other nuclei, Ref. [2]. In that work, 'good' fits are presented with the suggestion that proton scattering for the nuclei studied was well understood in terms of l-independent local potentials. However, the fitted data extended to only 70 degrees, and effects due to specific features of nuclear structure are expected to be most evident at large angles, see, e.g., Ref. [3].

The measurements of Ref. [2] present the opportunity of extending our previous work in two ways. Reference [1] mostly related to 30.3 MeV protons on ^{40}Ca, but included trends of significant properties up to 45 MeV. The 65 MeV measurements of Ref. [2] allow us to extend our understanding of pickup coupling to a somewhat higher energy and study the contribution of neutron pickup in a case where it is expected to be very large, i.e., for ^{48}Ca with its eight $7/2^-$ neutrons.

II. DYNAMIC POLARIZATION POTENTIAL

The contribution of reaction channel or inelastic couplings can be understood in terms of Feshbach's theory [4] which

———————
[*]raymond.mackintosh@open.ac.uk
[†]nicholas.keeley@ncbj.gov.pl

formally leads to a correction term to be added to a simpler form, notionally calculated by a folding model. The correction term is both complex (in both senses) and nonlocal in a way that is distinct from the well-understood nonlocality arising from exchange processes. The correction term also has a different form for each partial wave: an extreme example of angular momentum dependence. There have been few attempts to calculate such a term. The basic formalism, and the difficulty in relating the results to phenomenology, are presented in the work of Rawitscher [5]. The nonlocal and angular momentum dependent potential correction term will be referred to here as the formal dynamical polarization potential.

A simple approach [6] to determining the correction term due to coupling is to fit the elastic scattering angular distribution calculated in a coupled channel (CC) calculation and identify the correction term as the difference between the fitted potential and the elastic channel potential of the CC calculation. The determination of DPPs by OMP-fitting introduces all the limitations and prejudices of optical model fits, not least with regard to the imaginary spin-orbit term which we now know is essential.

In the present work the correction term is determined by subjecting the S matrix S_{lj}, that has been calculated in the CC calculation, to S matrix to potential inversion [7–10] and then subtracting the bare potential of the CC calculation. The resulting correction term is a local and l-independent representation of the formal dynamical polarization potential, DPP. The sum of this correction term and the bare potential is appropriate for comparison with both empirical local potentials and potentials resulting from most modern folding model calculations. However, it is significant that the correction term *is* a local representation of the formal nonlocal DPP. The nonlocality and also l dependence of the underlying formal DPP will have significant consequences that will be discussed in this paper. In this work, CC refers to any channel coupling, including coupled reaction channel (CRC) or continuum discretized coupled-channels (CDCC).

The two cases that we study are 65 MeV proton scattering from ^{48}Ca and ^{40}Ca. The angular distribution and analyzing power data for both of these cases have been fitted, Ref. [2], over a restricted angular range with conventional parametrized local potentials. The ^{48}Ca case is of particular interest because of the probable very strong neutron pickup coupling. It is expected to have characteristics that differ from the ^{40}Ca case. Our study of the ^{40}Ca case will also connect with our earlier ^{40}Ca work [1] at lower energies.

To determine local DPPs we first establish suitable bare potentials for CC calculations of 65 MeV proton scattering from ^{48}Ca and from ^{40}Ca. To do this we search for potential parameters that fit the elastic scattering angular distributions and analyzing powers when used in a CC calculation with coupling to all the reaction channels that are expected to contribute significantly to the DPP. Details of the channel couplings will be presented in Sec. III. The large effects of the coupling are evident in Fig. 1 for 65 MeV protons on ^{48}Ca and Fig. 2 for 65 MeV protons on ^{40}Ca. In these figures the solid lines represent CC fits to the angular distributions and analyzing powers with a bare potential optimized with both pickup and inelastic channels coupled. The fit to the data is
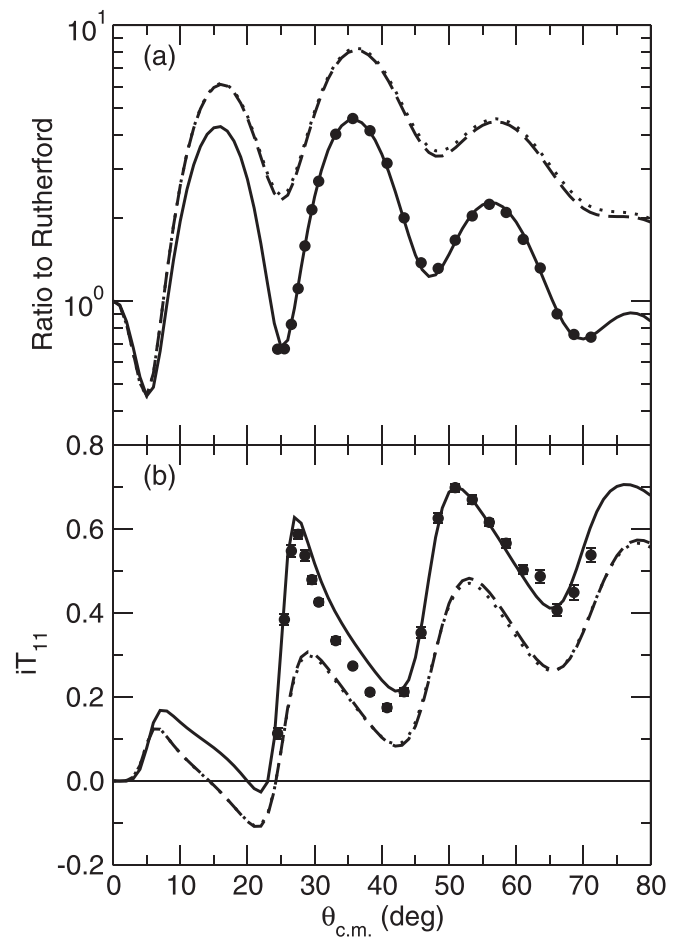

FIG. 1. For elastic scattering of 65 MeV protons on ^{48}Ca, the solid lines are the differential cross section (above) and analyzing power angular distributions for the full coupled channel calculation with fitted optical model parameters. The dotted lines are calculated with the same potential (the 'bare potential') but with no coupling. The barely visible dashed lines are for the bare potential plus inelastic coupling alone (no pickup).

quite good. The dotted lines represent the angular distribution and analyzing power without any channel coupling, that is, with the bare potential. The dashed lines in both figures represent the calculated observables with the bare potential when just the inelastic channels are coupled. These two figures show the dominance of pickup coupling over inelastic coupling for 65 MeV protons for both ^{48}Ca and ^{40}Ca. The very large contribution from pickup of a $7/2^-$ neutron to proton scattering from ^{48}Ca is evident in Fig. 1.

All DPP calculations presented herein employ the respective ^{40}Ca or ^{48}Ca bare potential determined in the above way. The use of fixed bare potentials, for the various different pickup and inelastic couplings that we study, is justified by the demonstration [11] that the DPPs are not very dependent on the bare potential.

III. REACTION CALCULATIONS

All reaction calculations employed the code FRESCO [12] and the inputs for ^{48}Ca and ^{40}Ca were kept as similar as
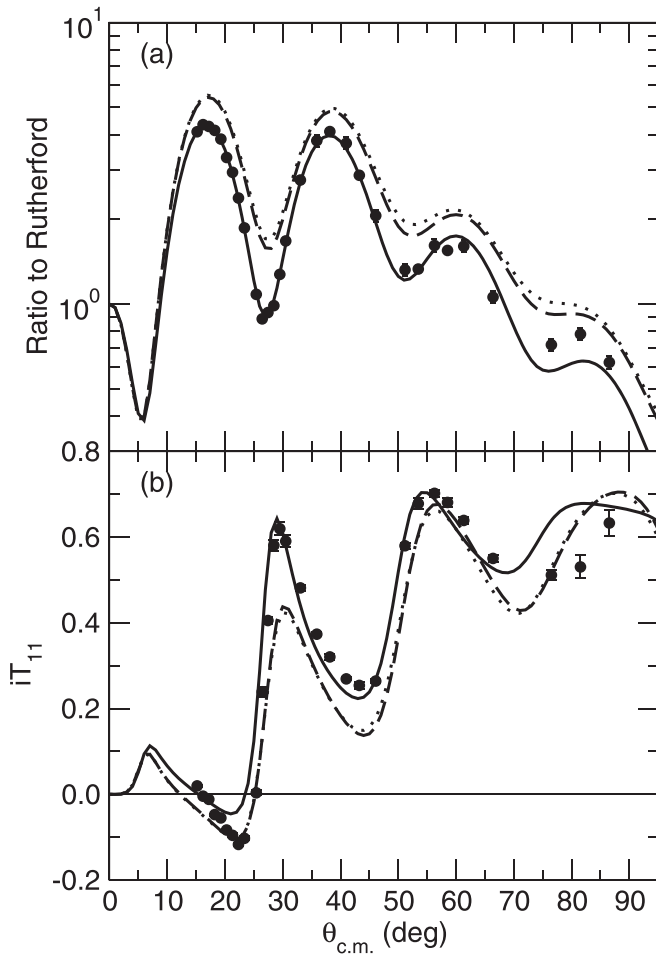
FIG. 2. For elastic scattering of 65 MeV protons on ^{40}Ca, the solid lines are the differential cross section (above) and analyzing power angular distributions for the full coupled channel calculation with fitted optical model parameters. The dotted lines are calculated with the same potential (the 'bare potential') but with no coupling. The dashed lines are for the bare potential plus inelastic coupling alone (no pickup).

possible, consistent with their different nuclear structures. The full coupling schemes for the two systems, $p + {}^{48}$Ca and $p + {}^{40}$Ca follow.

A. Inelastic couplings

For ^{48}Ca, inelastic couplings to the 4.507-MeV 3^- and 3.8317-MeV 2^+ levels were included using standard collective model form factors. The 2^+ coupling also comprised a reorientation term with the strength fixed according to the rotational model. The Coulomb coupling strengths were fixed using the recommended $B(E3)$ and $B(E2)$ values from Refs. [13,14], respectively. The nuclear deformation lengths, $\delta_3 = 0.6667$ fm and $\delta_2 = 0.50$ fm, were obtained by fitting the 65-MeV ^{48}Ca(p, p') inelastic scattering data of Fujita *et al.* [15].

For ^{40}Ca, inelastic couplings to the 3.737-MeV 3^- and 3.9044-MeV 2^+ levels were included, again using standard collective model form factors and with the 2^+ coupling

comprising a reorientation term according to the rotational model. Coulomb coupling strengths were also fixed using the appropriate recommended $B(E3)$ and $B(E2)$ values from Refs. [13,14], respectively. The nuclear deformation length for excitation of the 3^- level, $\delta_3 = 1.1925$ fm, was obtained by fitting the 65-MeV ^{40}Ca(p, p') inelastic scattering data of Ejiri *et al.* [16]. The corresponding deformation length for excitation of the 2^+ level, $\delta_2 = 0.45$ fm, was taken from Ref. [17]. The stronger coupling to the 3^- level for ^{40}Ca, reflected in the larger δ_3, corresponds to the greater difference between the dotted and dashed lines in Fig. 2 than in Fig. 1.

B. Pickup couplings

For ^{48}Ca pickup to the following levels of ^{47}Ca was included: the $7/2^-$ ground state, the 2.0135-MeV $3/2^-$ level, the 2.5783-MeV $3/2^+$ level, the 2.5995-MeV $1/2^+$ level, and the 3.425-MeV $7/2^-$ level. Spectroscopic factors and bound state form factors were taken from Schmitt and Santo [18]. In what follows where a single $7/2^-$ state is referred to, it is the ground state.

For ^{40}Ca pickup to the following four levels of ^{39}Ca was included: the $3/2^+$ ground state, the 2.467-MeV $1/2^+$ level, the 2.796-MeV $7/2^-$ level, and a $5/2^+$ level at 6.5132 MeV. This latter is a composite level containing the summed $5/2^+$ strength at the "center of gravity" excitation energy, weighted by the respective spectroscopic factors. These levels correspond to the "All1" set used in Ref. [1]. The form factors and spectroscopic factors were as in Ref. [1].

The $\langle d \mid n + p \rangle$ overlaps were calculated using the Reid soft-core potential [19] for both systems and included the small D-state component.

C. Optical potentials

The ^{48}Ca and ^{40}Ca proton optical potentials referred to in Sec. II were based on the corresponding optical model parameters of Sakaguchi *et al.* [2], adjusted to recover the fit to the corresponding elastic scattering data of Ref. [2] with the full (inelastic + pickup) coupling schemes using the SFRESCO search package [12]. In these calculations the exit channel deuteron potentials were calculated using the global optical model parameters of Daehnick *et al.* [20]. The resulting parameters are listed in Table I.

In order to investigate the effect of explicitly including breakup couplings in the deuteron exit partition, calculations were carried out with deuteron potentials obtained via Watanabe folding [21]. In what follows these will be referred to using the labels "PUBU(W)" and "PU(W)" for the calculations with and without breakup couplings, respectively. The PUBU(W) calculations all employed the same continuum model space, divided into bins of width $\delta k = 0.125$ fm^{-1} up to a maximum of $k_{\max} = 1.0$ fm^{-1}, where k is the momentum of the n-p relative motion. Relative angular momenta of $L = 0$ and 2 were included in the continuum and all allowed couplings up to multipolarity $\lambda = 2$. The folded diagonal and coupling potentials, including continuum-continuum couplings, were calculated using the central parts of the global nucleon-nucleus potential of Ref. [22]. While this potential

TABLE I. Optical potential parameters obtained by fitting the 65 MeV ^{48}Ca(p, p) (first row) and ^{40}Ca(p, p) (second row) elastic scattering data of Ref. [2] with the full (inelastic + pickup) calculations. Radii follow the convention $R_i = r_i \times A_t^{1/3}$ fm and $r_C = 1.25$ fm.

V	r_V	a_V	W	r_W	a_W	W_d	r_d	a_d	V_{so}	r_{so}	a_{so}
35.596	1.230	0.6934	3.727	1.191	0.7620	1.439	1.371	0.5466	5.523	1.177	0.6846
33.787	1.230	0.7165	4.508	1.153	0.7667	1.878	1.395	0.4575	4.571	1.088	0.6058

has been largely superseded by more recent work, e.g., CH89 [23] or that of Koning and Delaroche [24], we used the older set to facilitate an eventual comparison with the adiabatic model analysis of Matoba *et al.* [25] of the ^{40}Ca(p, d) reaction at 65 MeV which employed it. In fact, test calculations with Watanabe folded potentials based on the global parameter set of Koning and Delaroche [24] gave results for the elastic scattering that were graphically indistinguishable from those based on the potentials of Ref. [22] up to angles of $\theta_{c.m.} = 160°$, providing an *a posteriori* vindication of the use of the earlier parameter set. The necessary deuteron internal wave functions required by the folding procedure were calculated with the Reid soft-core potential [19], as used for the $\langle d \mid n + p \rangle$ overlaps.

In all the calculations which follow, the entrance channel potential parameters for a given system were fixed at the values listed in Table I, regardless of the particular set of channels included in the coupling scheme. The justification for using the same bare potential for all couplings, in the case of a particular target nucleus, was mentioned above.

IV. DPPS FOR 65 MeV PROTON ELASTIC SCATTERING ON ^{48}Ca

A. Evaluating the DPPs

The local equivalent DPPs for each coupling case are determined by subtracting the components of the bare potentials from the corresponding components of the potential determined by inverting S_{lj} for the elastic channel. Characteristic properties of the DPPs for various combinations of the possible couplings are presented in Table II as the differences between corresponding properties of the inverted and bare potentials.

Table II employs the standard normalization of Ref. [26] for J_R and J_{IM}, the volume integrals of the real and imaginary potentials. We apply the standard sign convention, in which a positive sign represents attraction or absorption. Thus, a negative value for ΔJ_R represents a repulsive contribution from the specified coupling. The tables also present Δ(CS), the change in reaction cross section due to the coupling. The quantity $\mathcal{R}$ is the ratio of Δ(CS) to ΔJ_{IM}, the change, due to coupling, in the volume integral of the imaginary central potential:

$$\mathcal{R} = \frac{\Delta(\text{CS})}{\Delta J_{IM}}. \tag{1}$$

The 'State CS' is the total (p, d) and/or (p, p') cross section in mb to the pickup states or collective states as specified in column 3. All calculations were carried out with a fixed bare potential. In Table II, (W) indicates deuteron Watanabe fold-

ing, see Sec. III C, PU indicates pickup and PUBU indicates breakup of the deuteron was included in the PU calculation.

B. Emerging regularities

We see from Table II that $\mathcal{R}$ varies over a much smaller range than either Δ(CS) or ΔJ_{IM} separately, relating the imaginary part of the DPP to the reaction cross section.

Less obvious, but possibly more informative, is the behavior of the quantity R_{CS}, defined as the ratio of Δ(CS) to State CS,

$$R_{CS} = \frac{\Delta(\text{CS})}{\text{StateCS}}. \tag{2}$$

There is a consistent difference between R_{CS} for pickup and inelastic coupling. For pickup coupling, the increase in reaction cross section, Δ(CS), greatly exceeds the State CS and R_{CS} thus greatly exceeds unity. However, for all cases of inelastic coupling, Δ(CS) is approximately the same as the State CS and R_{CS} is close to unity, line 7 of Table II (see also line 8 of Table III for the ^{40}Ca case). The values of Δ(CS) for pickup suggest that the pickup channels are acting as a 'doorway' to fusion and other processes. The differences in Q values, momentum transfers, etc., imply very different paths for the outgoing particles from inelastic or transfer coupling. (For the original doorway states, see for example, Ref. [27].)

In this work, we refer to cases for which $R_{CS} > 1$ as 'doorway-like' (DW) cases and those where $R_{CS} < 1$ as 'antidoorway' (ADW). For 30.3 MeV protons on ^{40}Ca pickup coupling leads to a DW effect with $R_{CS} \approx 10$. We remark that DW is predominant with transfer reactions involving protons, Ref. [1], but ADW appears to be predominant for inelastic excitations, and also for transfer reactions involving ^{3}He, Ref. [28], and ^{3}H, Ref. [29]. For further discussion, see Sec. VI.

C. Radial forms of the DPP for ^{48}Ca

Figure 3 compares the bare potential with the inverted potential that generates the S_{lj} when pickup coupling is included. The derived properties, DPPs, etc., of the potentials are in line 1 of Table II. Note the repulsive effect for r less than about 5 fm, and the extra absorption for r out to about 7 fm. The real spin-orbit term is not much modified except in the surface region. An imaginary spin-orbit term is generated. Subtracting the bare potential from specific inverted potentials will yield the DPPs to be presented below. The deuteron OMP for the cases in lines 1–9 of Table II is that of Daehnick *et al.* [20].

Figure 4 compares the DPP for three cases: the dotted lines are for pickup only (line 1, Table II), the solid lines are for both pickup and inelastic coupling together (line 8), and the dashed lines are for inelastic coupling only (line 7). Line 9 of

TABLE II. For proton scattering from ^{48}Ca at 65 MeV, volume integrals ΔJ (in MeV fm^3) of the DPP induced by (p, d) pickup coupling, 'PU', and/or coupling to inelastic states, 'Inel'. The coupled states for ^{48}Ca are given, with excitation energies, in Sec. IV. The ΔR_{rms} column gives the change in rms radius of the real central component (in fm). The final four columns present, respectively, the change in the total reaction cross section due to the coupling, the integrated cross section to specific coupled channels, the ratios $\mathcal{R}$ and R_{CS} defined in the text. Note that negative ΔJ_R corresponds to repulsion. The quantities $\Delta(CS)$ and State CS are given in mb. Note that the 47.62 mb for the state CS in the PUBU case (line 11) includes the continuum states of the deuteron. The CS to the bound deuteron is 16.59 mb. For the $3/2^+$ state in line 13, the CS to the bound deuteron is 2.22 mb, much less than the 11.88 mb which includes transitions to the continuum. For the 8.309 mb State CS in line 15, just 1.144 mb is for the deuteron bound state. The summed quantities in line 9 refer to PU in line 1 and Inel in line 7. The (W) in lines 10–15 indicates use of Watanabe folding, see text. Line 5 presents results of coupling only the states in lines 2 and 3; line 6 gives the sum of corresponding quantities in lines 2 and 3.

Line	Coupling	States	ΔJ_R	ΔJ_{IM}	ΔJ_{RSO}	ΔJ_{IMSO}	ΔR_{rms}	$\Delta(CS)$	State CS	$\mathcal{R}$	R_{CS}
1	PU	see text	−42.95	48.093	0.688	−0.817	0.0513	225.91	37.50	4.70	6.02
2	PU	$7/2^-$	−22.53	23.669	0.054	0.230	0.0101	139.80	28.25	5.91	4.95
3	PU	$3/2^+$	−9.59	6.504	0.467	−0.328	0.016	40.90	6.785	6.29	6.02
4	PU	$1/2^+$	−5.00	2.402	0.151	−0.026	0.0048	15.9	2.610	6.62	6.03
5	PU 2 state	$7/2^-, 3/2^+$	−34.47	38.06	0.563	−0.526	0.0363	196.55	34.65	5.16	5.67
6	PU summed	$7/2^-, 3/2^+$	−32.12	30.17	0.521	−0.098	0.0261	180.70	35.04	5.99	
7	Inel	$3^-, 2^+$	0.38	2.024	0.023	0.0007	0.0007	13.67	13.84	6.75	0.99
8	Inel and PU	see text	−42.63	50.217	0.647	−0.807	0.0549	234.85	48.63	4.68	4.83
9	Inel + PU	summed	−42.57	50.117	0.711	−0.816	0.0521	239.58	51.00	4.78	
10	PU (W)	$7/2^-$	−19.47	22.74	0.499	1.059	0.0008	137.01	29.82	6.02	4.39
11	PUBU (W)	$7/2^-$	−14.22	45.52	1.095	0.542	0.0092	240.25	47.62	5.28	5.05
12	PU (W)	$3/2^+$	−8.14	4.187	0.243	−0.063	0.0068	27.8	3.58	6.64	7.77
13	PUBU (W)	$3/2^+$	−12.27	12.93	0.237	−0.279	0.0202	79.77	11.88	6.17	6.71
14	PU (W)	$1/2^+$	−4.19	1.852	0.196	0.023	−0.0014	12.4	1.515	6.70	8.18
15	PUBU (W)	$1/2^+$	−6.78	6.323	0.201	−0.013	0.0064	42.3	8.309	6.66	5.09

TABLE III. For proton scattering from ^{40}Ca at 65 MeV; c.f. Table II. In line 12, of the State CS (4.382 mb), 1.549 mb was to the deuteron bound state (BS); line 14, of the State CS (9.298 mb), 2.879 mb was to the deuteron BS; in line 16, of the State CS (10.352 mb), 4.862 mb was to the deuteron BS, in line 19, of the State CS (14.773 mb), 4.480 mb was to the deuteron BS. In line 23, of the State CS (20.904 mb), 6.93423 mb was to the two states with the deuteron in its BS. No R_{CS} value is given for summed cases.

| Line	Coupling	States	ΔJ_R	ΔJ_{IM}	ΔJ_{RSO}	ΔJ_{IMSO}	ΔR_{rms}	$\Delta(CS)$	State CS	$\mathcal{R}$	R_{CS}
1	PU	see text	−19.45	24.94	0.700	−1.064	0.0552	100.53	20.782	4.031	4.84
2	PU	$1/2+$	−2.41	2.414	0.102	−0.034	0.0063	12.22	3.255	5.062	3.75
3	PU	$7/2-$	0.040	0.882	0.039	0.011	0.0021	4.809	1.104	5.423	4.36
4	PU	$3/2^+$	−7.32	7.885	0.461	−0.546	0.0212	37.24	8.136	4.723	4.58
5	PU	$5/2^+$	−7.00	7.575	0.110	0.0104	0.0177	37.14	7.534	4.903	4.92
6	PU both	$3/2^+, 5/2^+$	−15.65	18.237	0.614	−0.7830	0.0441	79.3	15.98	4.84	4.96
7	PU	summed	−14.32	15.46	0.571	−0.5356	0.0389	74.38	15.67	4.81	
8	Inel	see text	0.0060	3.888	0.0003	0.0144	−0.0015	21.28	21.528	5.473	0.99
9	Inel, PU	see text	−19.59	28.941	0.648	−1.067	0.0515	117.33	40.054	4.054	2.93
10	Inel + PU	summed	−19.44	28.828	0.7003	−0.92	0.0537	121.81	42.31	4.225	
11	PU(W)	$1/2^+$	−2.20	1.874	0.093	0.0082	0.0051	9.57	2.225	5.11	4.30
12	PUBU(W)	$1/2^+$	−3.17	4.001	0.125	−0.0085	0.0075	20.85	4.382	5.21	4.76
13	PU(W)	$3/2^+$	−6.83	5.26	0.283	−0.1339	0.0145	26.31	5.167	5.002	5.09
14	PUBU(W)	$3/2^+$	−10.01	12.274	0.305	−0.3208	0.0275	57.95	9.298	4.721	6.23
15	PU(W)	$5/2^+$	−5.93	6.888	0.203	0.220	0.0136	34.82	7.707	5.055	4.52
16	PUBU(W)	$5/2^+$	−7.83	13.521	0.353	0.210	0.0277	64.55	10.352	4.774	6.24
17	PU(W)	$1/2^+, 3/2^+$	−9.70	7.535	0.399	−0.160	0.0196	36.48	7.442	4.841	4.92
18	PU(W)	summed	−9.03	7.134	0.376	−0.1257	0.0196	35.88	7.392	5.020	
19	PUBU(W)	$1/2^+, 3/2^+$	−14.00	19.008	0.528	−0.4426	0.0374	84.01	14.773	4.420	5.69
20	PUBU(W)	summed	−13.28	16.275	0.430	−0.3293	0.0350	78.80	13.680	4.841	
21	PU(W)	$3/2^+, 5/2^+$	−13.63	13.442	0.571	0.293	0.0293	63.46	12.685	4.721	5.00
22	PU(W)	summed	−12.76	12.148	0.486	0.0861	0.0281	61.13	12.874	5.017	
23	PUBU(W)	$3/2^+, 5/2^+$	−13.50	30.514	0.564	−0.5312	0.0317	125.9	20.904	4.126	6.02
24	PUBU(W)	summed	−17.84	25.795	0.658	−0.1108	0.0552	122.5	19.650	4.749	
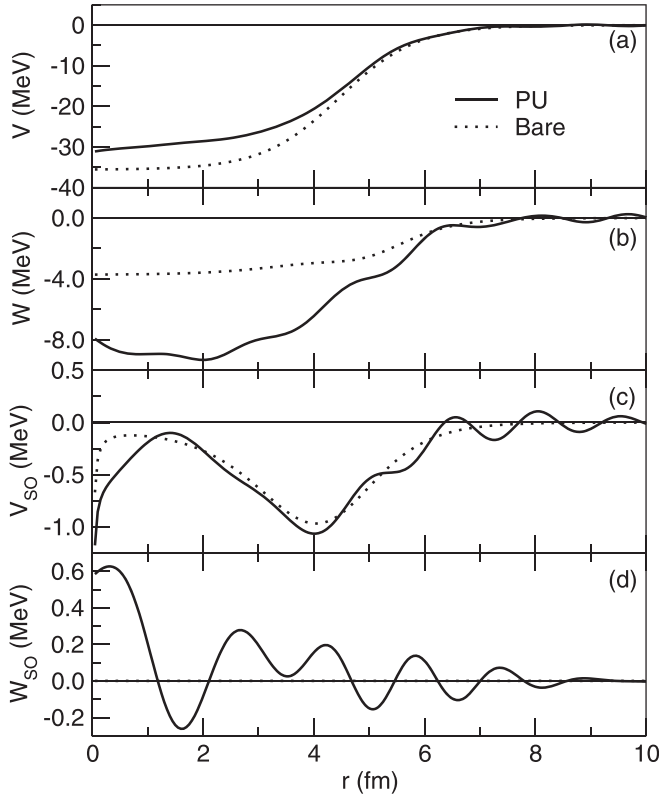
FIG. 3. For 65 MeV protons on ^{48}Ca, the dotted lines represent the bare potential and the solid lines represent the potential found by inversion for the full pickup calculation as in line 1 of Table II. The top panel (a) represents the real, central term, the second panel (b) the imaginary central term. Panels (c) and (d) are the real and imaginary spin-orbit terms, respectively.

Table II gives the numerical sums of the volume integrals of the pickup and inelastic DPPs. The differences between lines 8 and 9 are significant and will be discussed below. Although the inelastic coupling makes only a small contribution to the DPP, the State CS is not correspondingly small.

Lines 2, 3, and 4 present the results for pickup to single states: $7/2^-$, $3/2^+$, and $1/2^+$. These and lines 5 and 6 will be referenced below in connection with dynamical nonlocality.

The various DPP components exhibit different degrees of undularity, 'waviness', particularly visible in the small components. While some degree of undularity may be due to the inversion process, undularity is an established consequence of underlying l dependence. The formal DPP depends on the angular momentum as well being nonlocal [5]. For the relationship between angular momentum dependence and the undularity of the l-independent S-matrix equivalents, see Ref. [30].

D. Breakup of the deuteron

To show the effect of breakup (BU) we present in Table II characteristics of the DPPs due to pickup coupling to three particular states: the lowest energy $7/2^-$, $3/2^+$, and $1/2^+$ states, each without breakup (lines 10, 12, 14) and with
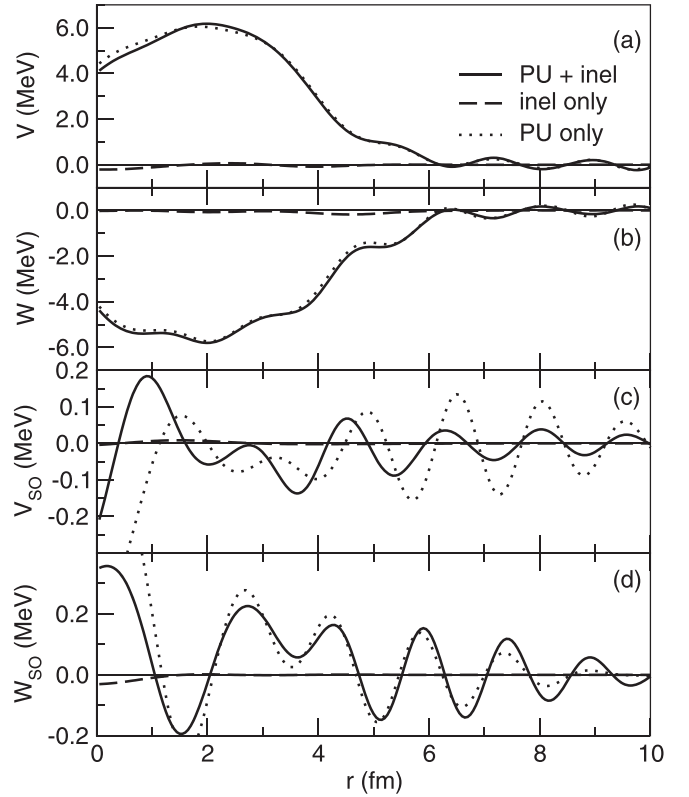

FIG. 4. For 65 MeV protons on ^{48}Ca, the dotted lines represent the DPP for pickup (PU) only, as in line 1 of Table II. The dashed lines represent the DPP for inelastic coupling, line 7 of Table II and the solid lines represent the DPP when pickup and inelastic coupling are both included, as in line 8 of Table II. The top panel (a) represents the real, central term, the second panel (b) the imaginary central term. Panels (c) and (d) are the real and imaginary spin-orbit terms, respectively.

breakup (lines 11, 13, and 15). The deuteron interaction is produced by Watanabe folding, indicated by (W), see Sec. III C. The DPPs corresponding to lines 10 and 11 together with the pickup DPP to the same states using the Daehnick deuteron OMP, line 2 are presented in Fig. 5. Comparison of the PU(W) and PUBU(W) cases reveals that the breakup of the deuteron following pickup has a large effect on the DPPs, particularly the imaginary terms, with a large increase in ΔJ_{IM}. The effect on $\mathcal{R}$ is relatively small. With breakup, in each case the cross section to bound deuteron channels is much smaller than the State CS. For example, the 47.62 mb for the state CS in the PUBU case (line 11) includes the continuum states of the deuteron and the CS to the bound deuteron is 16.59 mb. For the $3/2^+$ state in line 13, the CS to the bound deuteron is 2.22 mb, much less than the 11.88 mb which includes transitions to the continuum. For the 8.309 mb State CS in line 15, just 1.144 mb was for the deuteron bound state. It would be very challenging to get a quantitative experimental identification of the associated protons and neutrons. Comparison of the solid and dotted lines in Fig. 5 shows a reasonable agreement between the (Non-BU) pickup calculations with the Daehnick and folding model deuteron OMPs.
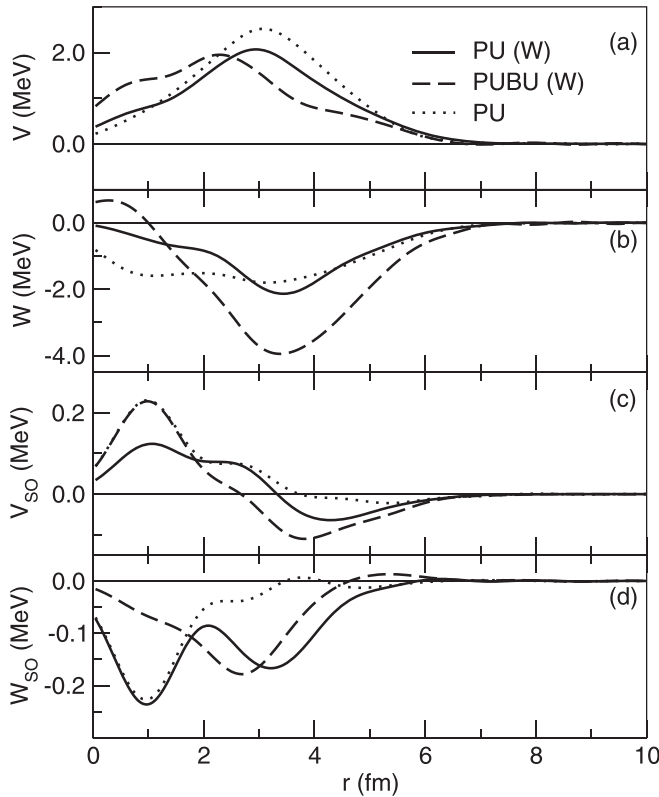
FIG. 5. For 65 MeV protons on ^{48}Ca, the solid lines represent the DPP found by inversion for cases with pickup coupling to the lowest $7/2^-$ state of ^{47}Ca as in lines 2, 10, and 11 of Table II. The solid lines represent the DPP in calculations based on Watanabe folding (see text). The dashed lines present the effect when deuteron breakup is included. The dotted line is for the DPP of line 2 of Table II employing the Daehnick deuteron potential. Panels (a)–(d) represent the real central term, the imaginary central term and the real and imaginary spin-orbit terms, respectively.

FIG. 6. For 65 MeV protons on ^{48}Ca, the solid lines represent the DPP found by inversion for the case of pickup coupling to the $7/2^-$ and $3/2^+$ states of ^{47}Ca as in line 5 of Table II. The dashed lines represent the numerical sum of the DPPs found by separate inversion for the cases of pickup coupling to the $7/2^-$ and $3/2^+$ states of ^{47}Ca as in line 6 of Table II. Panels (a)–(d) represent the real central term, the imaginary central term and the real and imaginary spin-orbit terms, respectively.

E. The dynamical non-locality of the DPPs for ^{48}Ca

The formal DPPs generated by coupling are nonlocal; the DPPs presented here are their local equivalents corresponding to the contribution of the particular couplings to the local OMP. Like most empirical OMPs, the outputs of local density model folding calculations are generally local and have rather smooth radial forms. Such local phenomenological OMPs are key ingredients in standard DWBA analyses of transfer reactions. Although there is now a considerable literature on exchange-generated nonlocality in direct reactions, the dynamically generated nonlocality is less discussed. In spite of its obvious significance for direct reactions, it has been little studied; for exceptions, see Refs. [31,32]. The dynamical nonlocality generated by the coupling to transfer and inelastic channels has a notable consequence. When several breakup or inelastic couplings are included, the formal dynamically nonlocal DPPs due to different couplings add to give the overall nonlocal DPP. However, this additivity does not apply to the local equivalents determined by inversion.

The local equivalent of a sum of nonlocal potentials is not the sum of the local equivalents of each separate nonlocal potential, see Refs. [31,32]. From this follows the nonadditivity
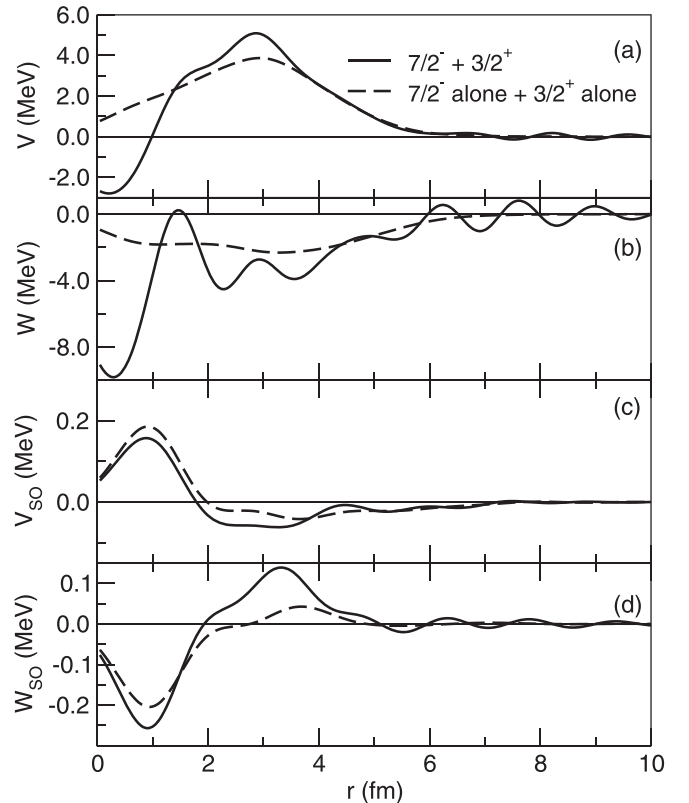
of the local DPPs found by inversion. This nonadditivity is clear evidence that the local DPPs presented here are local equivalents of the nonlocal DPPs generated by coupling; the formal nonlocal DPPs are additive. The nonadditivity of the local forms can be seen in comparisons of lines 5 and 6 and lines 8 and 9 of Table II. The first comparison, shown in Fig. 6, illustrates the nonadditivity of the local equivalent DPPs for two pickup states. The second comparison, shown in Fig. 7, reveals that the small local equivalent DPP due to inelastic scattering and the local equivalent pickup DPP do not sum to the DPP when both couplings are active. In particular this is the case for ΔJ_{IM} and $\Delta(CS)$.

A further consequence of dynamical nonlocality is the influence between channels that are not mutually coupled. One consequence is the nonadditivity of $\Delta(CS)$ where the values in lines 5 and 6 differ by 15.85 mb. This difference is not related to S-matrix inversion.

Six further cases of non-additivity will be presented in Table III for ^{40}Ca. The proton OMP evidently has a component that is nonlocal in a way that is distinct from exchange nonlocality, as was demonstrated long ago formally in Refs. [4,5]. That work also implied an angular momentum dependence in the DPP.
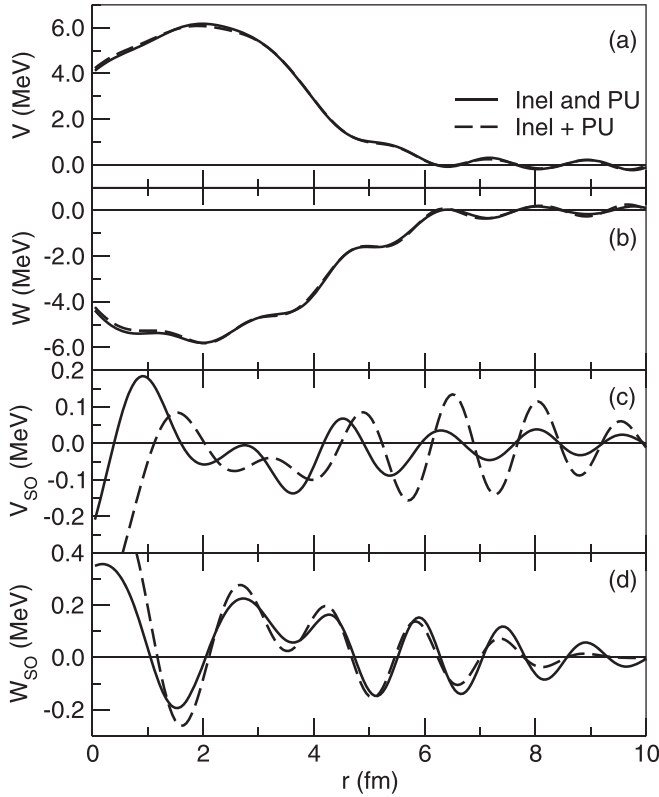
FIG. 7. For 65 MeV protons on ^{48}Ca, the solid lines represent the DPP found by inversion when pickup and inelastic coupling are both included. The dashed lines represent the numerical sum of DPPs calculated for pickup and inelastic coupling separately. Compare lines 8 and 9 of Table II. Panels (a)–(d) represent the real central term, the imaginary central term and the real and imaginary spin-orbit terms, respectively.

V. DPPS FOR 65 MeV PROTON ELASTIC SCATTERING ON ^{40}Ca

The effect of pickup coupling on the elastic scattering of 65 MeV protons on ^{40}Ca can be seen in Fig. 8. The difference between the pickup 'PU' and bare 'Bare' potentials does not extend to as large a radius (r) as for the ^{48}Ca case in Fig. 3, consistent with the fact that ΔJ_R and ΔJ_{IM} are both much smaller than for ^{48}Ca. The quantitative properties of the DPPs for 65 MeV protons on ^{40}Ca are given in Table III in the same format as Table II.

A. Radial forms of the DPP for ^{40}Ca

The repulsive and absorptive effects towards the nuclear center, evident in Fig. 8, are explicit in Fig. 9 which also shows the dominant effect of pickup compared to inelastic coupling. It also shows that the contributions do not add, as seen in the ^{48}Ca case. A significant imaginary spin-orbit term is generated, different in form from that for ^{48}Ca.

As was the case for ^{48}Ca, the breakup of the deuteron increases the magnitude of the real and imaginary central terms of the DPP. This is shown in Figs. 10 and 11. The dotted curves in these figures show the imperfect extent to which the
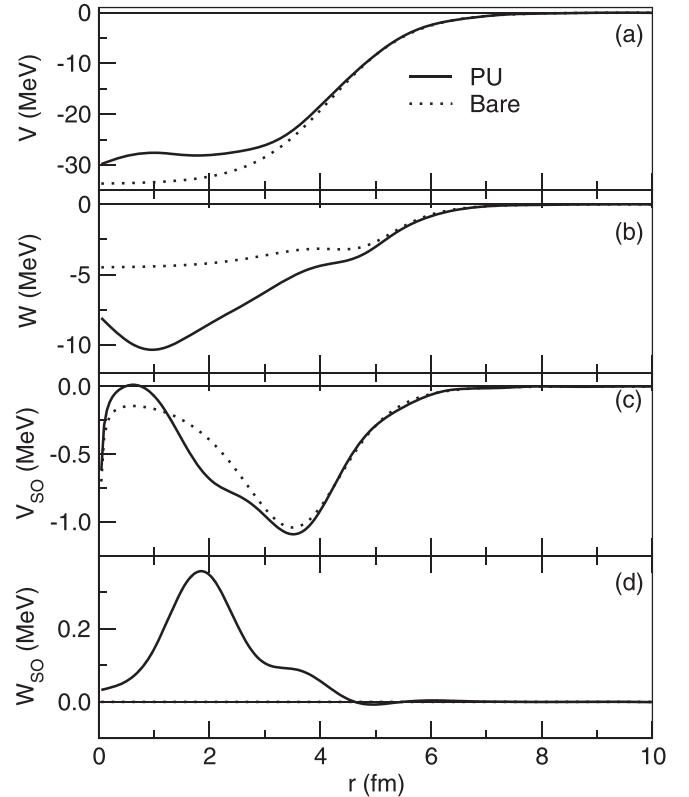

FIG. 8. For 65 MeV protons on ^{40}Ca, the dotted lines represent the bare potential and the solid lines represent the potential found by inversion for the full pickup calculation as in line 1 of Table III. The top panel (a) represents the real, central term, the second panel (b) the imaginary central term. Panels (c) and (d) are the real and imaginary spin-orbit terms, respectively.

pickup calculations employing the Daehnick deuteron OMP agree with the folding model calculations. These cases are generally similar but they reveal that it matters whether the coupled state has $j = l + \frac{1}{2}$ or $j = l - \frac{1}{2}$: it can be seen that coupling to the $5/2^+$ state of ^{39}Ca rather than the $3/2^+$ state leads to a reversal in the sign of the imaginary spin-orbit DPP.

Figures 10 and 11 both show how the breakup of the deuteron greatly enhances the pickup effect, especially in regard to the absorptive potential. This is in line with the value of R_{CS}. Note that the total effect of pickup coupling with breakup is much greater than for the coupling to the $3/2^+$ without deuteron breakup. Computational limitations did not allow breakup calculations with the full set of states, but there is no reason to suppose that the effect of breakup for all states would not follow the pattern in Fig. 11. For each case, the partial cross section to the deuteron bound state when breakup coupling was included was less than when there was no breakup (as was the case for ^{48}Ca).

B. The dynamical nonlocality of the DPPs for ^{40}Ca

We noted above the relationship between the nonadditivity of local DPPs and dynamical nonlocality. Figure 12 relates to lines 4 to 7 of Table III concerning pickup to the $3/2^+$ and $5/2^+$ states. The magnitude of the DPPs is considerably
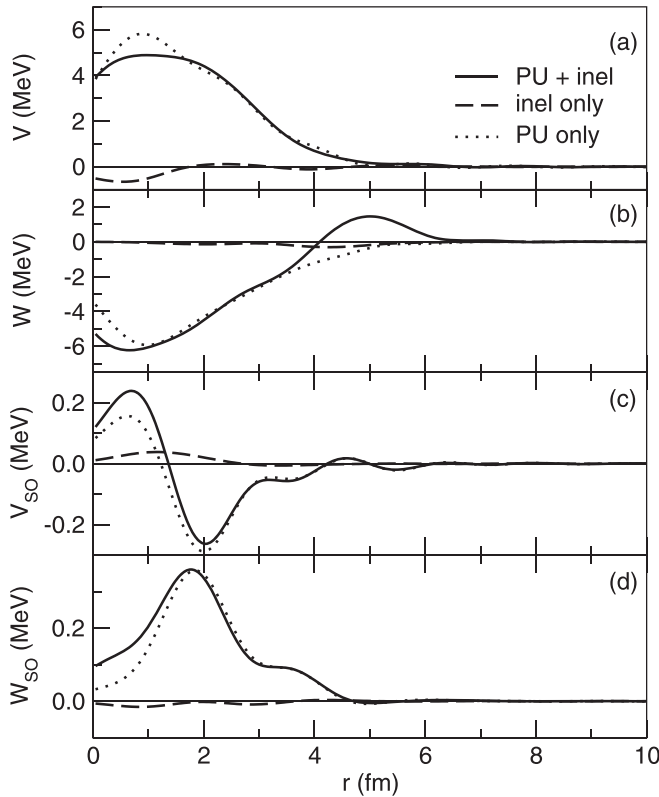
FIG. 9. For 65 MeV protons on ^{40}Ca, the dotted lines represent the DPP for pickup only, the dashed lines for inelastic coupling only and the solid lines for pickup and inelastic coupling; for lines 1, 8, and 9, respectively of Table III. The top panel (a) represents the real, central term, the second panel (b) the imaginary central term. Panels (c) and (d) are the real and imaginary spin-orbit terms, respectively.

FIG. 10. For 65 MeV protons on ^{40}Ca, the DPPs found by inversion for pickup coupling to the $5/2^+$ state of ^{39}Ca as in lines 5, 15, and 16 of Table III. The solid lines represent the DPP in calculations with the deuteron OMP based on Watanabe folding (see text) and the dashed lines present the effect when breakup is included in that calculation. The dotted line is for the DPP of line 5 of Table III with the Daehnick deuteron potential. Panels (a)–(d) represent the real central term, the imaginary central term, and the real and imaginary spin-orbit terms, respectively.

greater when both couplings are active together, solid lines, than the sum of the DPPs for independent coupling. This is a clear consequence of the dynamical nonlocality of the formal DPPs.

The nonadditivity of local DPPs applies also when the deuteron is subject to breakup, as shown in Fig. 13. In this case the 'together' DPPs have some indications of interference effects. The imaginary spin-orbit term exhibits a substantial difference.

VI. REGULARITIES IN R_{CS}

In many cases, channel coupling induces a much larger increase in the reaction cross section than in the cross section to the coupled state. The quantity R_{CS}, the ratio of Δ(CS) to the state cross section, is quite different for pickup coupling compared to inelastic coupling in a way that is the same for ^{40}Ca and ^{48}Ca at 65 MeV, as well as for ^{40}Ca at lower energies, see Ref. [1]. For inelastic coupling, unlike pickup coupling, R_{CS} is close to unity and the increase in reaction cross section is close to the inelastic scattering cross section.

Pickup coupling leads to a large increase in the reaction cross section: from Table II we see that for ^{48}Ca, pickup coupling increases the reaction cross section by a factor of 5 to 8 times the cross section to the pickup states. For ^{40}Ca,
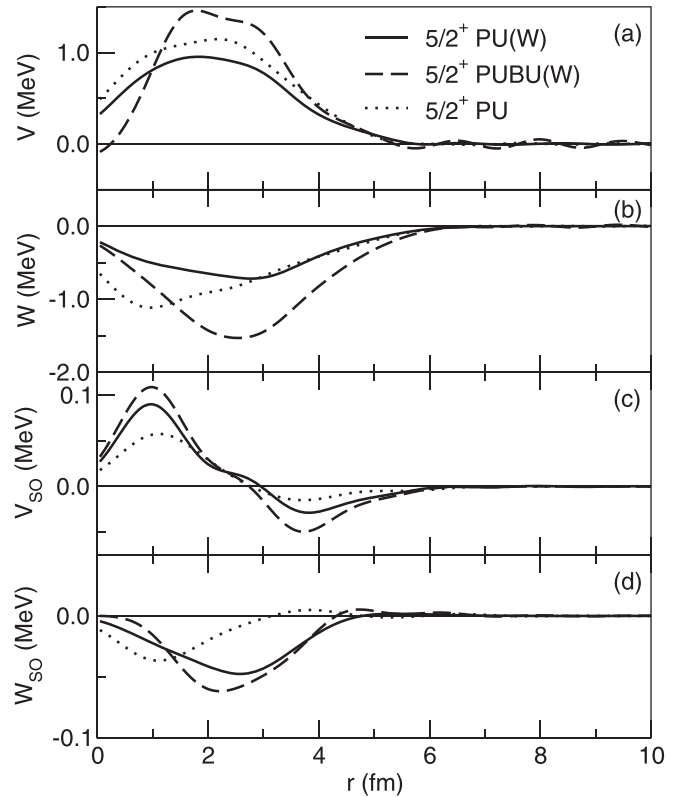
Table III reveals an increase by a factor of 4 to 7 times the pickup cross section. It is as if the pickup acts as a doorway to other processes, removing flux from the elastic channel. Cases where R_{CS} is significantly greater than unity have large values of ΔJ_{IM}. While breakup does have a considerable effect on both the state CS and Δ(CS), the ratio R_{CS} varies much less. The relatively small range of values of R_{CS} for either ^{40}Ca or ^{48}Ca over quite a large range of values of the cross section to the pickup states ('State CS') is as yet unexplained.

The earlier (p, d) pickup study for 30.3 MeV protons on ^{48}Ca [1] also included results at somewhat higher energies. The quantity R_{CS} for 30.3 MeV was 9.68; for 35 MeV R_{CS} was 7.32; for 40 MeV R_{CS} was 5.82, for 45 MeV R_{CS} was 4.96. This trend gives a reasonable match to the 65 MeV value of 4.84, line 1 of Table III. We would say that the doorway-like effect is large at 30.3 MeV, falling with increasing energy.

The doorway-like effect found for (p, d) coupling is not a universal property of pickup coupling in general. In a study of the pickup contribution to the ^{3}H OMP for 33 MeV ^{3}H on ^{48}Ca, we found $R_{CS} = 0.55$, Ref. [29]. For 33 MeV ^{3}He on ^{48}Ca, we found $R_{CS} = 0.71$ [28]. That is to say, the increase in the reaction cross section following pickup leading to ^{4}He was
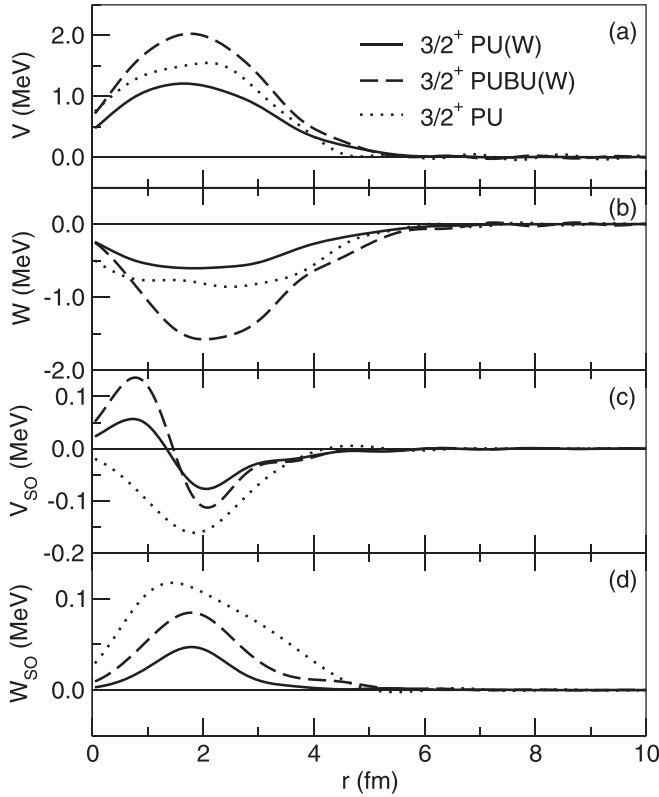
FIG. 11. For 65 MeV protons on ^{40}Ca, the solid lines represent the DPP found by inversion for pickup coupling to the $3/2^+$ state of ^{39}Ca as in lines 4, 13, and 14 of Table III. The solid lines represent the DPP in calculations with the deuteron OMP based on Watanabe folding (see text) and the dashed lines present the effect when breakup is included in that calculation. The dotted line is for the DPP of line 4 of Table III with the Daehnick deuteron potential. Panels (a)–(d) represent the real central term, the imaginary central term and the real and imaginary spin-orbit terms, respectively.

FIG. 12. For 65 MeV protons on ^{40}Ca, the dotted lines represent the DPP for pickup to the $3/2^+$ state, the dashed lines represent the DPP for pickup to the $5/2^+$ state, the solid lines pickup when coupling to both these states. The dot-dashed lines represent the numerical sum of the DPPs for the same two states. The relevant lines of Table III are 4, 5, 6, and 7, respectively. The top panel (a) represents the real, central term, the second panel (b) the imaginary central term. Panels (c) and (d) are the real and imaginary spin-orbit terms, respectively.

less than the pickup cross section, effectively an antidoorway effect. In these cases the Q value is positive; the interaction of the increased energy ^{4}He with the residual nucleus will be very different from that of a reduced energy ^{2}H. We note that in the two cases of inelastic coupling reported in Tables II (line 7) and III (line 8) $R_{CS} = 0.99$. Hence, in effect, the reaction cross section increases by the magnitude of the inelastic scattering cross section. This puts the very different behavior of the pickup cases in perspective.

The doorway-like effect, whereby R_{CS} is much greater than unity, was already noted in the early, primitive (zero range coupling etc), study of pickup coupling in proton scattering [33].

VII. COMPARISON WITH GLOBAL POTENTIAL

It is instructive to compare the difference between the ^{40}Ca and ^{48}Ca derived potentials when pickup coupling is included with the same difference according to a global potential. The Koning Delaroche (KD) global potential [24] reflects the general expectation that increasing neutron numbers lead to a proton OMP with a deeper real central term. Thus, for the
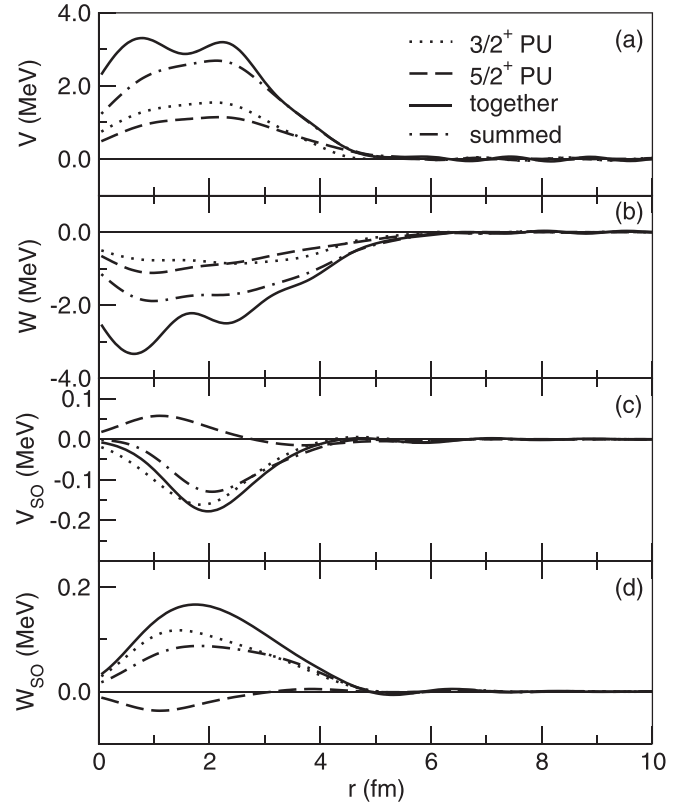
KD OMP, the normalized volume integral of the real potential, J_R, is 8.9 MeV fm^3 greater for ^{48}Ca than for ^{40}Ca. However, for the Sakaguchi real OMP, fitted to their elastic scattering data, the normalized volume integral of the real potential, J_R, is 18.6 MeV fm^3 *less* for ^{48}Ca than for ^{40}Ca. In the present work, the fits to the same data shown in Figs. 1 and 2 led to a normalized volume integral of the real potential, J_R, that is 18.3 MeV fm^3 *less* for ^{48}Ca than for ^{40}Ca, closely matching the Sakaguchi result. This match is enabled by the fact that the full repulsive effect of the coupling (see line 8 of Table II and line 9 of Table III) is much greater for ^{48}Ca than for ^{40}Ca. For ^{48}Ca, $\Delta J_R = -42.63$ MeV fm^3 compared to -19.59 MeV fm^3 for ^{40}Ca. Thus the strong repulsive effect of the pickup coupling perfectly explains the departure from the global OMP prediction for the real part of the ^{48}Ca OMP.

There is a similar, if not quite as exact, reproduction of the departure from the global trend in the imaginary part: the KD global potential predicts the volume integral of the imaginary term to be just 1.57 MeV fm^3 greater for ^{48}Ca than for ^{40}Ca. For the Sakaguchi potential, a greater difference of 6.65 MeV fm^3 is found. Our CRC pickup model predicts an even greater
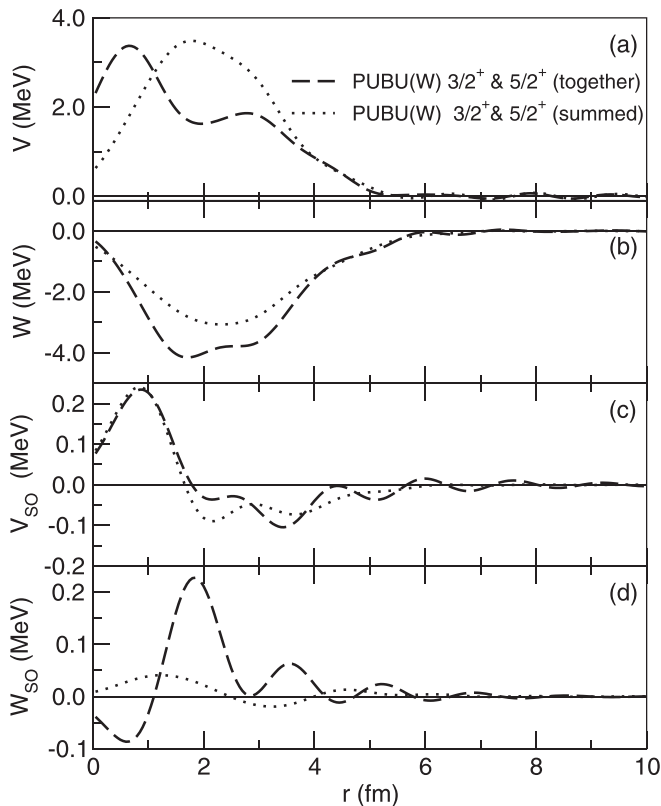
FIG. 13. For 65 MeV protons on ^{40}Ca, the DPPs for calculations for pickup coupling to the $3/2^+$ and $5/2^+$ states of ^{39}Ca with the deuteron OMP based on Watanabe folding together with breakup of the deuteron, comparing the sum of the DPPs as in lines 14, 16 of Table III with the DPP when both states are coupled together, as in line 23 of Table III. The dashed lines represent the DPP when $3/2^+$ and $5/2^+$ states are both coupled and the dotted lines represent the sum of the DPPs for coupling to the $3/2^+$ and $5/2^+$ states separately. Panels (a)–(d) represent the real central term, the imaginary central term and the real and imaginary spin-orbit terms, respectively.

difference of 11.98 MeV fm^3. Computational limitations did not permit comparisons of full ^{40}Ca and ^{48}Ca cases including breakup.

In summary, Sakaguchi's OM fit and the present CRC+inversion calculations including pickup agree that the ^{48}Ca real central OMP is substantially shallower than predicted by the KD global potential, and also predicted by the regular increase in depth of the proton OMP with neutron excess.

VIII. COMMENT ON DYNAMICAL NONLOCALITY

In Secs. IV E and V B we presented evidence for dynamical nonlocality for 65 MeV protons on ^{48}Ca and ^{40}Ca. This was based primarily on the demonstrated nonadditivity of local DPPs. However, there is more general evidence, for example the fact that the cross section to particular states is influenced by other states that are included in the coupling scheme but not coupled to the states in question. This is exemplified in various cases of the nonadditivity of the State CS values as, for example, in lines 17 to 24 of Table III. This result is

not dependent on the inversion of S_{lj}. Also not dependent on inversion is the fact that the coupling induced change in the reaction cross section Δ(CS) when two states are coupled is not the sum of the Δ(CS) values for each state separately. This can be seen in the Δ(CS) column in Table III lines 6 and 7, lines 9 and 10, lines 17 to 24. with similar cases in Table II.

Further discussion of dynamical nonlocality is given in Ref. [32]. In particular, direct evidence was presented in a comparison of DWBA calculations for (p, d) reactions in which the proton OMP was calculated in two ways: (1) dynamically nonlocal due to coupling to vibrational states of the target nucleus, and, (2) the local equivalent to this potential, as determined by inversion. In the case of 65 MeV protons on ^{48}Ca, where coupling to vibrational states is not strong, the most feasible test of that kind would be a DWBA (p, d) calculation comparing angular distributions with the proton wave function calculated in two ways: (1) nonlocal as a result of coupling to pickup channels with and without breakup, and (2) the S-matrix equivalent local potential determined by inversion. This will be the subject of a subsequent publication.

IX. SUMMARY AND CONCLUSIONS

The simplest direct reaction, elastic scattering, receives a substantial contribution from the coupling between the elastic channel and reaction channels, specifically (p, d) coupling. This challenges any model of nucleon-nucleus scattering, like that of Ref. [34], that entails just a single nucleon in the continuum. Such models may well be valid at much lower energies but certainly not for 65 MeV protons. Moreover, the radial form of the DPPs presented here has no clear representation in local density folding models.

Previously, Ref. [1], the importance of (p, d) coupling was shown for 30.3 MeV protons on ^{40}Ca, with further results for a series of higher energies. Although the pickup contribution falls with increasing energy, we have shown that it is still substantial for 65 MeV protons. Particular pickup effects for 65 MeV protons on ^{40}Ca follow the energy dependent trend of Ref. [1]. As expected, the DPP, particularly the absorptive component, is much greater for ^{48}Ca than for ^{40}Ca owing to the pickup of a $7/2^-$ neutron. The DPPs for proton scattering from ^{40}Ca and ^{48}Ca are very different in magnitude; no smoothly varying global OMP could fit proton scattering from both ^{40}Ca and ^{48}Ca. Accounting for departures from global OMPs is challenging and will certainly involve CRC contributions among others. It is reasonable to suppose that the processes studied here will have some representation in future nuclear calculations beyond the standard nucleon model of nuclei.

Coupling to deuteron channels is far from the only process contributing to nucleon elastic scattering. Others will generate different characteristic departures from global models. A complete description, including exchange, of elastic nucleon-nucleus scattering remains a major challenge for theory and experiment. The problem cannot be considered solved until neutron scattering is also fully accounted for, something that is not on the horizon in view of the almost total absence of relevant neutron analyzing power measurements.

[1] N. Keeley and R. S. Mackintosh, Phys. Rev. C **99**, 034614 (2019).

[2] H. Sakaguchi, M. Nakamura, K. Hatanaka, A. Goto, T. Noro, F. Ohtani, H. Sakamoto, H. Ogawa, and S. Kobayashi, Phys. Rev. C **26**, 944 (1982).

[3] P. E. Hodgson, *Nuclear Reactions and Nuclear Structure* (Clarendon Press, Oxford, 1971), p. 201.

[4] H. Feshbach, Ann. Phys. (NY) **5**, 357 (1958); **19**, 287 (1962).

[5] G. H. Rawitscher, Nucl. Phys. A **475**, 519 (1987).

[6] R. S. Mackintosh, Nucl. Phys. A **164**, 398 (1971).

[7] R. S. Mackintosh and A. M. Kobos, Phys. Lett. B **116**, 95 (1982).

[8] S. G. Cooper and R. S. Mackintosh, Inverse Probl. **5**, 707 (1989).

[9] V. I. Kukulin and R. S. Mackintosh, J. Phys. G **30**, R1 (2004).

[10] R. S. Mackintosh, Scholarpedia **7**, 12032 (2012).

[11] R. S. Mackintosh and N. Keeley, Phys. Rev. C **98**, 024624 (2018).

[12] I. J. Thompson, Comput. Phys. Rep. **7**, 167 (1988).

[13] T. Kibédi and R. H. Spear, At. Data Nucl. Data Tables **80**, 35 (2002).

[14] S. Raman, C. W. Nestor, Jr., and P. Tikkanen, At. Data Nucl. Data Tables **78**, 1 (2001).

[15] Y. Fujita, M. Fujiwara, S. Morinobu, T. Yamazaki, T. Itahashi, H. Ikegami, and S. I. Hayakawa, Phys. Rev. C **37**, 45 (1988).

[16] H. Ejiri, M. Sasao, T. Shibata, H. Ohsumi, Y. Fujita, M. Fujiwara, T. Yamazaki, I. Katayama, S. Morinobu, and H. Ikegami, Phys. Rev. C **24**, 2001 (1981).

[17] R. S. Mackintosh and N. Keeley, Phys. Rev. C **90**, 044601 (2014).

[18] D. Schmitt and R. Santo, Z. Phys. **233**, 114 (1970).

[19] R. V. Reid, Jr., Ann. Phys. (NY) **50**, 411 (1968).

[20] W. W. Daehnick, J. D. Childs, and Z. Vrcelj, Phys. Rev. C **21**, 2253 (1980).

[21] S. Watanabe, Nucl. Phys. **8**, 484 (1958).

[22] F. P. Becchetti, Jr. and G. W. Greenlees, Phys. Rev. **182**, 1190 (1969).

[23] R. L. Varner, W. J. Thompson, T. L. McAbee, E. J. Ludwig, and T. B. Clegg, Phys. Rep. **201**, 57 (1991).

[24] A. J. Koning and J. P. Delaroche, Nucl. Phys. A **713**, 231 (2003).

[25] M. Matoba, O. Iwamoto, Y. Uozumi, T. Sakae, N. Koori, T. Fujiki, H. Ohgaki, H. Ijiri, T. Maki, and M. Nakano, Phys. Rev. C **48**, 95 (1993).

[26] G. R. Satchler, *Direct Nuclear Reactions* (Clarendon Press, Oxford, 1983).

[27] N. Austern, *Direct Nuclear Reaction Theories* (Wiley-Interscience, New York, 1970), pp. 368–370.

[28] R. S. Mackintosh and N. Keeley, Phys. Rev. C **100**, 064613 (2019).

[29] N. Keeley and R. S. Mackintosh, Phys. Rev. C **102**, 064611 (2020).

[30] R. S. Mackintosh, Eur. Phys. J. A **55**, 147 (2019).

[31] R. S. Mackintosh and N. Keeley, Phys. Rev. C **81**, 034612 (2010).

[32] N. Keeley and R. S. Mackintosh, Phys. Rev. C **90**, 044602 (2014).

[33] R. S. Mackintosh, Nucl. Phys. A **230**, 195 (1974).

[34] C. Mahaux and H. A. Weidenmüller, *Shell-Model Approach to Nuclear Reactions* (North-Holland, Amsterdam, 1969).